
A Possible Origin of KHz QPOs in Low-Mass X-ray Binaries

Shoji KATO¹ and Mami MACHIDA²

¹2-2-2 Shikanodai-Nishi, Ikoma-shi, Nara 630-0114, Japan

²Department of Physics, Faculty of Science, Kyushu University, 744 Motoooka, Nishi-ku, 819-0395, Japan

*E-mail: kato.shoji@gmail.com, mami@phys.kyushu-u.ac.jp

Received (reception date); Accepted (acceptation date)

Abstract

A possible origin of kHz QPOs in low-mass X-ray binaries is proposed. Recent numerical MHD simulations of accretion disks with turbulent magnetic fields of MRI definitely show the presence of two-armed spiral structure in quasi-steady state of accretion disks. In such deformed disks, two-armed ($m = 2$) c-mode ($n = 1$) oscillations are excited by wave-wave resonant instability. Among these excited oscillations, the fundamental in the radial direction ($n_r = 0$) will be the higher kHz QPO of a twin QPOs, and the first overtone ($n_r = 1$) in the radial direction will be the lower kHz QPO of the twin. A possible cause of the twin high-frequency QPOs (HFQPOs) in BH X-ray binaries is also discussed.

Key words: accretion, accretion disks — instabilities — kHz QPOs: binaries— waves — X-rays: binaries

1 Introduction

The origin of quasi-periodic oscillations (QPOs) in low-mass X-ray binaries is one of controversial problems. One of their possible origins will be disk oscillations. There is, however, no

¹ 2-2-2 Shikanodai-Nishi, Ikoma-shi, Nara 630-0114, Japan

² Department of Physics, Faculty of Science, Kyushu University, 744 Motoooka, Nishi-ku, 819-0395, Japan

definite disk oscillation model which explains why particular modes of oscillations are excited and appear as QPOs. One of promising mechanisms for explaining them is the warp resonant model (Kato 2004, 2008; Ferreira and Ogilvie 2008; Otkarian et al. 2010). In this model, the unperturbed disk is assumed to have been deformed from an axisymmetric state by a warp. Through the warp, two particular oscillation modes are resonantly coupled and excited (a kind of three mode coupling). In this resonant instability, one of the excited oscillation modes is axisymmetric g-mode.¹ This axisymmetric g-mode oscillation is self-trapped in the inner region of disks, and is regarded as one of quasi-periodic oscillations.

In the case where disks have poloidal magnetic fields this self-trapping of g-mode oscillations is questioned by Fu and Lai (2009). Dewberry et al. (2018), however, show that this sensitivity of the trapping to poloidal magnetic fields is weakened if toroidal magnetic fields of moderate strength are present. Based on this consideration, Dewberry et al. (2019a,b) developed the resonant model to cases of magnetized disks, focusing on eccentric disks as well as warped disks.

The above-mentioned warp resonant instability can be interpreted as a particular case of a more general resonant instability (Kato 2013, 2014). The latter instability is called here and hereafter "wave-wave resonant instability in deformed disks". The instability condition can be expressed in a quite simple form (Kato 2013). For this resonant instability to work, the disk deformation required is not restricted only to a warp (and eccentric deformation), but also other types of disk deformations are allowed, if there are disk oscillation modes which satisfy necessary instability conditions. A typical example is the 3 : 1 tidal instability (Kato 2013).

In a binary system the disk around the primary star is tidally deformed. In tidally deformed disks a disk instability which is called the 3 : 1 resonance occurs (Whitehurst 1988; Hirose and Osaki 1990; Lubow 1991). In a viewpoint of particle approximation, the instability is a parametric resonance (Hirose and Osaki 1990). In a viewpoint of fluid systems the cause of this instability is explained by a mode-mode coupling of perturbations (Lubow 1991). In the viewpoint of the wave-wave resonant instability mentioned above, this 3 : 1 resonance is a particular example of the instability of the above-mentioned wave-wave resonant instability in a deformed disks (Kato 2013).

The disk deformations expected in disks surrounding compact objects are not limited to warped nor tidal ones. MHD simulations of accretion disks with MRI turbulence show that the magnetized accretion disks are not axisymmetric in quasi-steady states, but have spiral

¹ The another terminology of g-mode is r-mode.

structure (Machida and Matsumoto 2008). Recently, much higher resolved MHD simulations of accretion disks by use of CANS+ (Matsumoto et al. 2019) show definitely the presence of spiral structures (Machida et al. in preparation). Then, a natural question is whether high-frequency disk oscillations observed in X-ray binaries can be explained as the oscillations excited by the wave-wave resonant instability through this disk deformation. The purpose of this paper is to examine this possibility and to suggest that kHz QPOs observed in low-mass X-ray binaries will be c-mode oscillations excited by this resonance process. Observational evidence shows that the high-frequency kHz QPOs observed in neutron-star X-ray binaries often appear in pair and their frequency changes in time are correlated (e.g., Belloni et al. 2003). This characteristics of correlated change of the pair QPOs is in favor of the idea that the oscillations are two-armed c-mode ones, as will be shown in the text.

In this paper, we first outline the essence of the wave-wave resonant instability in deformed disks formulated by Kato (2013, 2016), and summarize the conditions of resonance and resonant instability. Then, we apply this instability to the case where the unperturbed disks are deformed from an axially-symmetric ones by a two-armed slowly rotating pattern. The results show that two-armed c-mode oscillations are excited, if they are reflected back outwards around the inner edge of the disks. Furthermore, we demonstrate that the magnitude of excited frequencies and their time correlated changes seem to qualitatively agree with those of twin kHz QPOs observed in low mass X-ray binaries.

Finally, a possible origin of high frequency QPOs (HFQPOs) observed in black-hole binaries is briefly discussed from a viewpoint of the wave-wave resonant instability in two-armed deformed disks.

2 Outline of Wave-Wave Resonance Instability

Before presenting an outline of the wave-wave resonant instability, we shall briefly classify the oscillation modes in geometrically thin relativistic disks. Then, we describe conditions of the resonant interaction and the resonant instability.

2.1 Wave Modes in Disks

Let us consider geometrically thin axisymmetric relativistic disks surrounding compact objects. To describe perturbations on the disks, we introduce cylindrical coordinates (r, φ, z) whose origin is at the center of the central object and the z -axis is perpendicular to the disk plane.

If the disk is approximated to be isothermal in the vertical direction (z -direction) and the

small amplitude perturbations superposed on axisymmetric disks are local in the radial direction (r -direction) in the sense that their radial wavelength is shorter than the characteristic radial scale of disks. Then, the dispersion relation describing the perturbations can be written as (e.g., Okazaki et al. 1987)

$$[(\omega - m\Omega)^2 - \kappa^2][(\omega - m\Omega)^2 - n\Omega_\perp^2] = k^2 c_s^2 (\omega - m\Omega)^2, \quad (1)$$

where perturbations have been taken to be proportional to $\exp[i(\omega t - m\varphi - kr)]$, ω is the frequency of perturbations, m the azimuthal wavenumber ($|m| = 0, 1, 2, 3, \dots$), k the wavenumber in the radial direction. $\Omega(r)$ is the angular velocity of disk rotation, taken to be Keplerian one $\Omega_K(r)$. In equation (1), κ and Ω_\perp are horizontal and vertical epicyclic frequencies, respectively, and c_s is the acoustic speed in disks. In the Newtonian disks, κ and Ω_\perp are equal to Ω_K , but in relativistic ones we have $\kappa(r) < \Omega_\perp(r) < \Omega_K(r)$ (e.g., Kato 2001). The symbol $n (= 0, 1, 2, 3, \dots)$ in equations (1) represents the node number of perturbations in the vertical direction. If $n = 0$, the oscillations have no mode in the vertical direction in the sense that there is approximately no vertical motion, i.e., the oscillations are nearly horizontal. In the case of $n = 1$, there is vertical motion crossing the equatorial plane.

It is noted that we consider nonself-gravitating relativistic disks, but the effects of general relativity are taken into account only by adopting general relativistic expressions for Ω_K , κ , and Ω_\perp . In others, Newtonian equations are adopted.

The oscillation modes are classified by m and n . The dispersion relation (1) gives two solutions with respect to $(\omega - m\Omega)^2$. In the case of $n = 0$, however, one of them is trivial, i.e., $(\omega - m\Omega)^2 = 0$, and the other is

$$(\omega - m\Omega)^2 = \kappa^2 + k^2 c_s^2. \quad (2)$$

This is the dispersion relation for inertial acoustic oscillations. In the case of $n \geq 1$, since Ω_\perp is always larger than κ , the two solutions with respect to $(\omega - m\Omega)^2$ of dispersion relation (1) are characterized by

$$(\omega - m\Omega)^2 < \kappa^2 \quad (3)$$

and

$$(\omega - m\Omega)^2 > n\Omega_\perp^2. \quad (4)$$

The former mode is g mode (it is also called r-mode), while the latter is called c-mode (corrugation mode) when $n = 1$, and vertical p-mode when $n \geq 2$.²

² In many previous papers written by Kato the latter mode with $n = 1$ are all called vertical p-mode except when $m = 1$; i.e., only the mode with $n = 1$ and

2.2 Conditions of Resonant Interaction

Let us assume that the unperturbed disks are deformed from an axisymmetric equilibrium state by a wavy perturbation. The perturbation is assumed to be time-periodic with frequency ω_D and azimuthal wavenumber m_D . On such deformed disks, two small-amplitude normal mode oscillations are superposed. The set of frequency and azimuthal wavenumber, (ω, m) , of these two normal mode oscillations are (ω_1, m_1) and (ω_2, m_2) . If there are the following resonant relations:

$$\omega_1 + \omega_2 + \omega_D = 0, \quad m_1 + m_2 + m_D = 0, \quad (5)$$

the two oscillations with (ω_1, m_1) (called hereafter mode 1) and (ω_2, m_2) (called hereafter mode 2) resonantly interact each other through the disk deformation with (ω_D, m_D) (called mode D). This is a kind of three mode resonant coupling.

One more relation is necessary for the resonant coupling. In idealized disks with vertically isothermal stratification, the variable $h_1 (\equiv p_1/\rho_0)$ (p_1 is pressure perturbation and ρ_0 is unperturbed density in disks) associated with disk oscillations with vertical node number n is proportional to $\mathcal{H}_n(z/H)$, i.e., $h_1 \propto \mathcal{H}_n(z/H)$ (e.g., Kato 2001, 2016), where \mathcal{H}_n is the Hermite polynomial of index n with argument z/H , H being the vertical scale length of disks. If an oscillation mode with n_1 nonlinearly couples with a disk deformation with $n_D = 0$, the resulting mode is an oscillation with n_1 . If the disk deformation has $n_D = 1$, however, the oscillation resulting from the nonlinear coupling is $\mathcal{H}_{n \pm 1}(z/H)$. Hence, for mode 1 and mode 2 to couple each other through a disk deformation of $n_D = 1$, the relation $n_2 = n_1 + 1$ or $n_2 = n_1 - 1$ is necessary. In summary, the additional resonant condition is

$$\begin{aligned} n_2 = n_1; & \quad \text{when } n_D = 0 \\ n_2 = n_1 + 1 \quad \text{or} \quad n_2 = n_1 - 1; & \quad \text{when } n_D = 1, \end{aligned} \quad (6)$$

where n_1 , n_2 , and n_D are the vertical node numbers of mode 1, mode 2, and the mode of disk deformation, respectively.

Finally, it should be noted that for three modes (mode 1, mode 2 and mode D) to have a nonlinear coupling, their radial propagation regions should be overlapped. Otherwise, there is no nonlinear coupling.

$m = 1$ was called c-mode. Here, however, all the latter mode with $n = 1$ is called c-mode irrespective of the value of m . The terminology of vertical p-mode is used for modes of $n \geq 2$. This classification has been used in Kato (2016).

2.3 Conditions of Resonant Instability

All conditions mentioned in subsection 2.2 are necessary for resonant coupling among three modes. We assume that the disk deformation mode (mode D) has a large amplitude compared with other two disk oscillation modes and is maintained by some excitation processes which are not considered here. Then, two modes (mode 1 and mode 2) are resonantly amplified or damped by the resonant coupling. The condition of resonant amplification is found to be written in a simple and general form. That is, the condition of amplification is (Kato 2013, see also Kato 2016)

$$\left(\frac{E_1}{\omega_1}\right)\left(\frac{E_2}{\omega_2}\right) > 0, \quad (7)$$

where E_1 and E_2 are wave energies of mode 1 and mode 2, respectively.³ This instability condition is quite general and valid even in magnetized disks (Kato 2014).

3 Two-Armed Deformed Disks and Excitation of Two-Armed C-mode Oscillations

For the wave-wave resonant instability outlined in section 2 to work, the unperturbed disks need to be deformed. Here, we consider the case where the disk is deformed by two-armed pattern. The wave-wave resonant instability known up to the present by other types of disk deformation will be briefly summarized in Appendix.

3.1 Presence of Two-Armed Pattern in Disks

Recently, high-resolution numerical MHD simulations of accretion disks have been done (Machida et al. in preparation), where angular momentum is transported by turbulence of magneto-rotational instability (MRI). The pseudo-Newtonian potential is used. The initial states of the systems are almost the same as those adopted by Machida et al. (2003, 2006).⁴ That is, the initial disk is a torus with horizontal magnetic fields of 100 plasma β ($\beta \equiv p_{\text{gas}}/p_{\text{mag}}$). The numbers of mesh points in the radial, azimuthal, and vertical directions are $(N_r, N_\varphi, N_z) = (774, 512, 774)$ in the maximum cases. The mass of the central source is $10M_\odot$.

The simulation results clearly show that the disks in the quasi-steady state are not axisymmetric, but spirally deformed. Figure 1 shows an example of density distributions on

³ An expression for wave energy E for normal mode oscillations is presented, for example, in Kato (2001, 2016). A simple expression for E is equation (3.31) in Kato (2016).

⁴ In Machida et al. (2003) the center of the initial torus was at $50r_S$, while in the new simulations it is at $40r_S$. In Machida et al. (2006) the temperature of the initial torus was slightly lower than that in the new simulations.

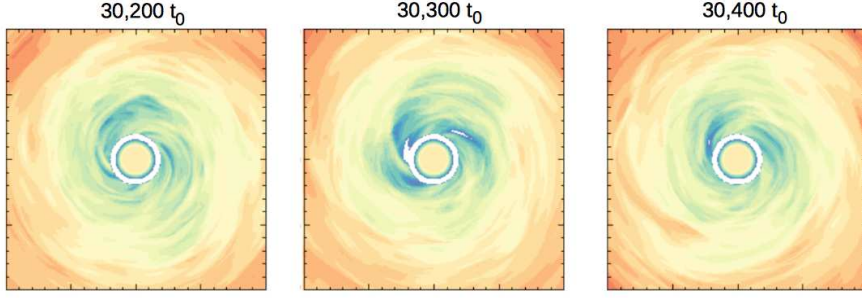


Fig. 1. Density distribution on the equatorial plane at epochs of $t = 3.02 \times 10^4 t_0$, $t = 3.03 \times 10^4 t_0$, $t = 3.04 \times 10^4 t_0$, where t_0 is the unit time defined by the Schwarzschild radius r_S and the speed of light c , i.e., $t_0 = r_S/c$. The radius of the central circle is $3r_S$. Comparison of the three panels shows that the spiral pattern rotates slowly in the prograde direction. (calculated from the data of Machida et al 2020)

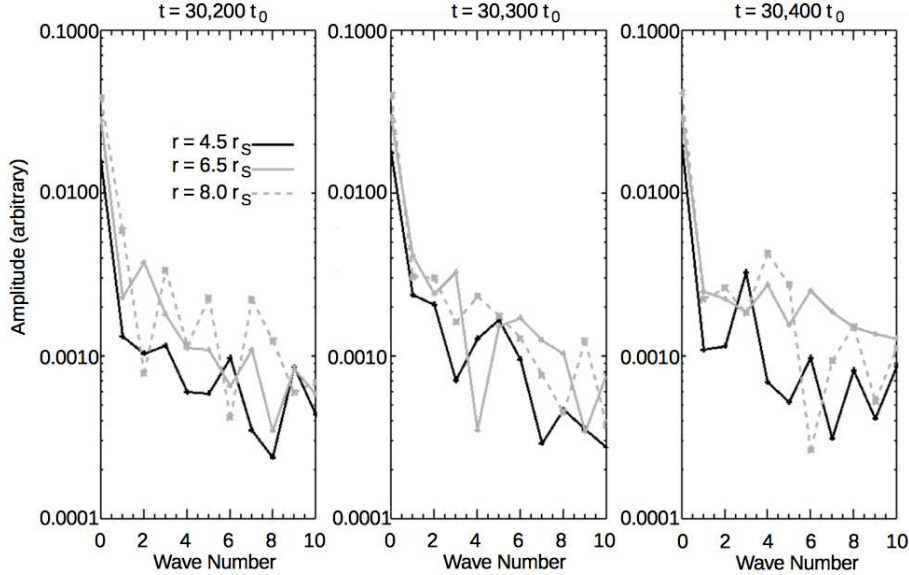


Fig. 2. The Fourier components of density variations in the azimuthal direction at radii of $r = 4.5r_S$, $6.5r_S$, and $8.0r_S$. The density averaged in the azimuthal direction is normalized to be unity. The abscissa denotes azimuthal wavenumber m . (calculated from the data of Machida et al 2020)

the equatorial plane with less spatial resolution of mesh points (774, 64, 774). Three epochs of $3.02 \times 10^4 t_0$, $3.03 \times 10^4 t_0$, and $3.03 \times 10^4 t_0$ are shown, where t_0 is the unit time defined by the Schwarzschild radius r_S and the speed of light c , i.e., $t_0 = r_S/c$. Comparison of the above three panels seems to show that the spiral pattern rotates slowly in the direction of disk rotation, but the angular velocity of the pattern rotation is much slower than that of the disk rotation. The spiral pattern has many arms. In order to see the strength of each arm, the density variation in the azimuthal direction is Fourier-analyzed at a few radius. The results are shown in figure 2 for $r = 4.5r_S$, $6.5r_S$, and $8.0r_S$. This figure shows that the amplitude of spiral density pattern over the averaged one is roughly a few to ten percent in density. The pattern of $m = 2$ is

certainly present, although it is not the most dominant one. What we need here is the $m = 2$ component.⁵

The origin of spiral disk deformation is an interesting subject, but here we simply assume that on the unperturbed disks a plane-symmetric, low-frequency two-armed pattern is present and maintained. That is, we assume the presence of a low-frequency, two-armed spiral pattern of

$$m_D = -2, \quad n_D = 0, \quad \text{and} \quad \omega_D \sim 0, \quad (8)$$

where we have adopted $m_D = -2$ (not $m_D = 2$) for convenience, because there is no essential difference between waves of $\exp[i(\omega_D t - m_D \varphi)]$ and those of $\exp[-i(\omega_D t - m_D \varphi)]$.

3.2 Mode 1 and Mode 2 Satisfying Resonant and Excitation Conditions

As two waves which resonantly interact through the above disk deformation, we consider the following set of two oscillations modes:

$$\text{mode 1: } c\text{-mode oscillations with } (m_1 = 2, n_1 = 1, \omega_1), \quad (9)$$

$$\text{mode 2: } c\text{-mode oscillations with } (m_2 = 0, n_2 = 1, \omega_2 \sim -\omega_1). \quad (10)$$

The issue to be examined next is whether the instability condition (7) is satisfied by the above oscillation modes. The propagation region of mode 1 specified by equation (9) is given by $(\omega_1 - 2\Omega)^2 > \Omega_\perp^2$ [see inequality (4)], which is divided into two regions of $\omega_1 > 2\Omega + \Omega_\perp$ and $\omega_1 < 2\Omega - \Omega_\perp$. We are interested in the oscillations in the latter propagation region, which is schematically shown in figure 3. The oscillation in this latter propagation region has a negative wave energy, since the propagation region is inside the corotation radius of $\omega = 2\Omega$.⁶ Hence, we have $E_1/\omega_1 < 0$. Next, we consider the c-mode oscillation specified by equation (10). The propagation region of the oscillations is specified by $\omega_2^2 > \Omega_\perp^2$ [see inequality (4)]. This propagation region consists of two domains, i.e., $\omega_2 > \Omega_\perp$ and $\omega_2 < -\Omega_\perp$. We are interested in the oscillations in the region of $\omega_2 < -\Omega_\perp$, which is also schematically shown in figure 3. This oscillation is axisymmetric and thus the wave energy is positive, leading to $E_2/\omega_2 < 0$, since $\omega_2 < 0$. Hence, the condition of resonant instability (7) is satisfied.

It is noted that the condition of resonance in frequency, i.e.,

⁵ In the present excitation model of kHz QPOs, the presence of a low-frequency two-armed pattern is essentially necessary. The presence of other components has no effects on our model, because they do not contribute to the resonance.

⁶ The sign of wave energy E of an oscillation with ω and m , $\text{sign}(E)$, is the same as the sign of $\omega(\omega - m\Omega)$ in the propagation region of the oscillation (e.g. see Kato 2016), i.e., $\text{sign}(E) < 0$ if $\omega/m < \Omega$, while $\text{sign}(E) > 0$ if $\omega/m > \Omega$. In other words, we have $\text{sign}(E) < 0$ inside the corotation radius of $\omega/m = 0$, while $\text{sign}(E) > 0$ outside the corotation radius of $\omega/m = 0$.

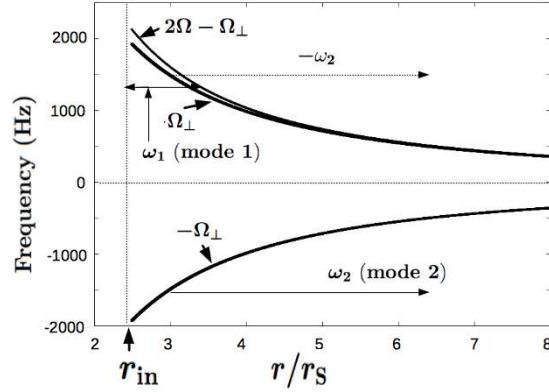


Fig. 3. Schematic figure showing one of propagation regions of two-armed c-mode oscillations (called mode 1) and one of propagation regions of axisymmetric p-mode oscillations (called mode 2). It is noticed that the propagation region of mode 1 is limited inside by the inner edge of the disks, r_{in} , and outside by the radius where $\omega_1 = 2\Omega - \Omega_{\perp}$. That is, the oscillation is trapped and has a discrete frequency. Different from this, the propagation region of mode 2 is limited inside by the radius where $-\omega_2 = \Omega_{\perp}$, but there is no explicit outer boundary. That is, the frequency of ω_2 is determined passively by the resonance condition. The curves of Ω_{\perp} and $2\Omega - \Omega_{\perp}$ in this diagram are drawn in the case of spin parameter a_* is 0.3 in order to demonstrate the difference of Ω_K and Ω_{\perp} .

$$\omega_1 + \omega_2 + \omega_D = 0 \quad (11)$$

is satisfied by adopting ω_2 so that the above resonant condition among frequencies holds for given ω_1 and ω_D . This is always possible, because mode 2 has practically no definite outer boundary (see figure 3). In other words, mode 2 is not a trapped oscillation.

In the present case the signs of ω_1 and ω_2 are opposite, because ω_D is smaller than ω_1 . Hence, the condition of resonant instability (7) can be written as $E_1 E_2 < 0$. This has a simple physical interpretation. That is, the resonant interaction of two oscillations with opposite signs of wave energy leads to instability by a positive energy flowing to the oscillation with positive energy from the one with negative energy.

It should be noticed that since ω_1 and $-\omega_2$ are close (ω_D is small), the outer edge (radius) of the propagation region of mode 1 and the inner edge of the propagation region of mode 2 are close (see figure 3), even when they are not overlapped. In the evanescent regions of oscillations, the amplitude of the oscillations spatially damps but it is still large near the boundary of the propagation region. Consequently, the necessary condition that the propagation regions of mode 1 and mode 2, and the disk deformation region are overlapped is practically satisfied.

4 Frequencies of Excited Oscillation Modes and kHz QPOs

Here, we examine whether the set of mode 1 and mode 2 considered above can describe the frequency of a kHz QPO. First, we should consider the frequency ω_1 of mode 1. To obtain ω_1

a boundary condition is necessary at an inner part of the disks. This is, however, a difficult subject, because we do not know what boundary condition can be imposed at the inner edge r_{in} of disks. (If we state more critically, it is uncertain whether we can impose a boundary condition near r_{in} .) Near the inner edge of the disks, r_{in} , the gas density decreases sharply towards the central source. Hence, a simple consideration suggests that Lagrangian pressure variation vanishes there, i.e., $\delta p = 0$ at r_{in} . However, we should consider that the accretion disks have inward flows and they become supersonic beyond the sonic point. In other words, the reflected waves are swallowed to the central object unless their outward wave velocity is sonic or more. A measure whether the reflected wave can go actually outwards against the inward accretion flow will be to compare the group velocity of the c-mode waves at r_{in} , c_c , with acoustic speed c_s . A rough estimate of c_c under the use of the local dispersion relation (1) shows that c_c is smaller than c_s near r_{in} . This suggests that there is no reflection of the c-mode oscillations at r_{in} .

However, we should consider following situations. The disk thickness $H(r)$ near r_{in} decreases sharply towards r_{in} . That is, $dH(r)/dr < 0$ with a large negative value. A direct effect of this decrease of disk thickness on wave motions will be their reflection outwards before approaching to r_{in} . This reflection may occur favorably for c-mode oscillations, because c-mode oscillations extend in the vertical direction, i.e., $p_1/\rho_0 \propto \mathcal{H}_1(z/H) \propto (z/H)$ in the case of local approximations with $dH/dr = 0$, where \mathcal{H}_n is the Hermite polynomial with index n . (It is noted that $p_1/\rho_0 \propto \mathcal{H}_0(z/H) \propto (z/H)^0$ in p-mode oscillations.) It is further noticed that the c-mode oscillations are nearly incompressible motions, i.e., $\delta\rho \sim 0$ (see e.g., Kato et al. 2008 or Kato 2016), and thus will be reflected on a discontinuous surface. Second, the effects of sharp decrease of disk thickness are not considered in deriving the dispersion relation (1). The sharp decrease of disk thickness and strong (MRI) turbulence will introduce modification of oscillation modes and their couplings, which will bring about reflection of oscillations.⁷ Taking the above situations into account, we impose in this paper a boundary condition at r_{in} , which is $p_1/\rho_0 = 0$ for simplicity.⁸

By imposing this condition as the inner boundary condition and by imposing the radius

⁷ In the case of p-mode oscillations, wave reflection (and instability) near the sonic point is known (e.g., Matsumoto et al. 1988; Kato et al. 1988; Honma et al. 1992). This is related to adoption of a diffusion-type viscous force (information can be transported through the sonic point outwards) or topology around the sonic point (e.g., nodal-type critical point), and might not be directly related in the present subject.

⁸ For comparison, a case where $\partial(p_1/\rho_0)/\partial r = 0$ is adopted as the inner boundary condition has been examined (Kato 2011). The value of ω_1 is quantitatively different from that in the case of $p_1/\rho_0 = 0$ (see figure 5 in Kato 2011), but there is no qualitative difference in the trend on the frequency-frequency curve given in figure 5 below.

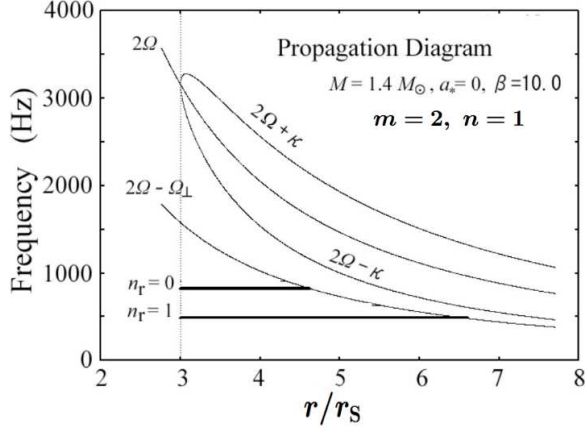


Fig. 4. Propagation diagram for two-armed c-mode oscillations ($n = 1$) with $n_r = 0$ and $n_r = 1$. The horizontal lines show the radial range where the oscillations are trapped. The disk temperature c_s is taken so that $\beta[\equiv c_s^2/(c_s^2)_0] = 10.0$ [see equation (12) for $(c_s^2)_0$]. $M = 1.4 M_{\odot}$ and $a_* = 0$ are adopted. (reproduced from Kato 2016)

where $\omega_1 = 2\Omega - \Omega_{\perp}$ as a turning point of the wave equation, Kato (2012b) solved the local wave equation⁹ describing oscillations by the WKB method to estimate the frequency of mode 1. The frequency ω_2 is determined by the resonance condition of $\omega_1 + \omega_2 + \omega_D = 0$. It is important to note here that mode 2 will not be observed clearly, since the oscillation is an outgoing running wave (see figure 3) (not a trapped one) and will be phase-mixed. That is, the oscillation of ω_1 alone is observed as a kHz QPO. This situation is the same as that in the case of superhumps (see Kato 2013).

The next issue is why kHz QPOs are often observed in pairs. It should be emphasized that the trapped c-mode oscillation with $m_1 = 2$ and $n_1 = 1$ (mode 1) has overtones resulting from node number(s) in the radial direction. The fundamental oscillation in the radial direction has no node in the radial direction, i.e., $n_r = 0$. This oscillation will correspond to the higher frequency QPO of a twin, and the lower frequency QPO will be the first overtone oscillation with $n_r = 1$. This idea that the two-armed c-mode oscillations with $n_r = 0$ and $n_r = 1$ are the pair of kHz QPOs is already suggested by Kato (2012b), but at that time we have no definite idea concerning excitation of these modes. Figure 4 demonstrates the trapping of c-mode oscillations with $n_r = 0$ and $n_r = 1$ on the propagation diagram in the case of a non-rotating central object.

Here, the main results by Kato (2012b) are presented. In his calculations, the disk temperature was taken as a parameter. As the reference temperature he adopted the temperature in the standard disks where gas pressure dominates over radiation pressure and opacity comes from the free-free processes. Furthermore, the conventional viscosity parameter, α , and the

⁹ This wave equation is the one derived under approximation of a constant disk thickness, and corresponds to the dispersion relation (1).

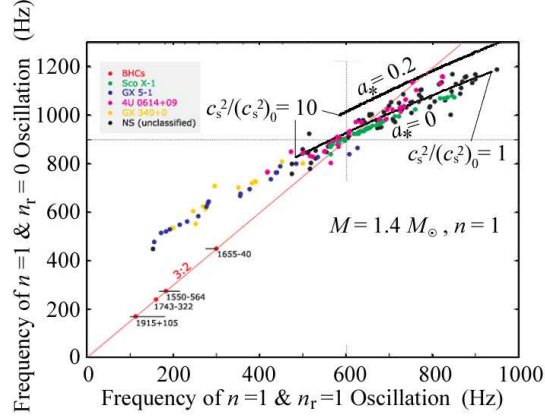


Fig. 5. Frequencies and their correlation between two-armed c-mode ($n = 1$) oscillations with $n_r = 0$ and $n_r = 1$ for two cases of $a_* = 0$ and 0.2 . The value of $c_s^2/(c_s^2)_0$ is changed from 1.0 to 10.0 . $M = 1.4M_\odot$ is adopted. The calculated curves are superposed on a figure by Abramowicz (2005) showing observational data on the frequency-frequency diagram. (The ordinate is the lower frequency of twin QPOs, and the abscissa is the higher frequency of the twin QPOs.) Original plots of observational data are those by Belloni et al. (2005). [Reproduction of Figure 5 in Kato (2012)]

mass accretion rate normalized by the Eddington critical accretion rate are taken, respectively, to be 0.1 and 0.3 . That is, as the reference isothermal acoustic speed, $[c_s(r)]_0$, he adopted

$$[c_s^2(r)]_0 = 1.79 \times 10^{16} \left(\frac{M}{M_\odot} \right)^{-1/5} \left(\frac{r}{r_S} \right)^{-9/10} \text{ cm}^2 \text{ s}^{-2}, \quad (12)$$

where M is the mass of the central source and r_S is the Schwarzschild radius, defined by $r_S = 2GM/c^2$.

Kato adopted $\beta_s [\equiv c_s^2/(c_s^2)_0]$ as a dimensionless parameter for describing the disk. The value of β_s will change in time by changes of accretion rate \dot{M} and viscosity parameter α . Since the trapped region of oscillations is narrow in the radial direction, β_s is taken to be a constant parameter independent of r . For some values of parameter β_s , the frequencies of trapped oscillations for the fundamental mode in the radial direction ($n_r = 0$) and those for the first overtone ($n_r = 1$) have been calculated. An example of his calculated results is shown in figure 5, which is a reproduction of figure 5 by Kato (2012b). This figure shows the correlated frequency change (by the change of β_s) of the fundamental ($n_r = 0$) and the first overtone ($n_r = 1$) on the frequency-frequency diagram. On this diagram frequencies of the observed higher and lower kHz QPOs are over-plotted. This figure shows that the calculated values of ω for $n_r = 0$ and $n_r = 1$ are in the observed frequency range of twin kHz QPOs and also their changes by change of c_s^2 qualitatively agree with the observed correlated change of twin QPOs.

Finally, the effects of magnetic fields on the above arguments are mentioned. Even if magnetic fields are present in disks, the expression for the wave-wave resonant instability condition, $(E_1/\omega_1)(E_2/\omega_2) > 0$, is kept unchanged (Kato 2014), although E_1 and E_2 are wave

energies where the effects of magnetic fields are taken into account. In addition, in the cases where magnetic fields in the unperturbed state are horizontal, the behaviors of c-mode oscillations on the frequency-frequency diagram qualitatively agree with observations (Kato 2012a). That is, Kato (2012a) examined the effects of magnetic fields in the horizontal direction on the c-mode oscillations with $m = 2$. In this study the magnetic fields in the horizontal direction are assumed to be stratified in the vertical direction so that the Alfvén speed is constant in the vertical direction (i.e., $B_0^2 \propto \rho_0$). Even in such simplified cases the wave equation describing the c-mode oscillations is complicated to solve directly by the WBKJ method. Hence, in that paper the oscillations are assumed to be nearly vertical and the motions in the radial direction associated with the oscillations are treated as a perturbation over the vertical motions (this approximation is valid in the case of c-mode oscillations with short radial wavelength). The results show that the calculated frequency-frequency correlation curve is qualitatively on the curve representing the trend of observed correlation, although the frequency range obtained by the calculations is changed from that in the case of no magnetic fields (for detail, see figures in Kato 2011).

5 Summary and Discussion on HF QPOs in BH X-ray binaries

Recent high-resolution MHD numerical simulations of accretion disks with high plasma β ($\equiv p_{\text{gas}}/p_{\text{mag}}$), starting from tori with toroidal magnetic fields, show that accretion disks surrounding compact objects with high plasma β are not axially symmetric in quasi-steady state, but have spiral structures (Machida et al. in preparation). Although the structure is complicated, spectrum analyses show a stiff presence of two-armed slowly progressive structure. Elucidation of the origin of the structure is of interest, but here we simply assume that the structure is maintained on the disks by some MHD precesses. That is, we assume the presence of disk deformation of ($m_{\text{D}} = 2, n_{\text{D}} = 0$) with a low frequency of ω_{D} . Then, high-frequency, two-armed c-mode oscillations of $m = 2$ and $n = 1$ are excited by the wave-wave resonance instability studied by Kato (2013, 2014), if the modes are reflected back outwards around the inner edge of the disks. We suggest that their fundamental mode ($n_r = 0$) in the radial direction and the first overtone ($n_r = 1$) are, respectively, the upper and the lower kHz QPOs observed in low-mass X-ray binaries.

A weak point of the present model of kHz QPOs is whether the c-mode oscillations are actually reflected back near the inner edge of the disks. Careful two-dimensional analyses of wave motions in accreting flows will be necessary in future. If wave reflection actually occurs

as is expected in this paper, comparisons of calculated frequencies and observed ones will be helpful for knowing the structure around the innermost region of disks (discoseismology).

In this paper high-frequency QPOs (HFQPOs) of black hole sources were outside of our main interest, because their observational characteristics are different from those of kHz QPOs of neutron-star X-ray binaries. That is, the twin HFQPOs in black-hole sources have a frequency ratio close to 3 : 2 and are almost time-independent, unlike the kHz QPOs. It is of interest to discuss why the HFQPOs in black-hole X-ray binaries are different in their characteristics from those in kHz QPOs in neutron stars, and whether they can be interpreted by the wave-wave resonant instability model. In the followings, we try to discuss the origin of the twin HFQPOs in the framework of the wave-wave resonant model.

The neutron stars in low-mass X-ray binaries are generally old, and thus the accretion disks surrounding the neutron stars will not have strong poloidal magnetic fields. In the case of BH binaries, however, the central part of accretion disks may be subject to poloidal magnetic fields of the central BH sources. In such cases, the propagation regions of wave modes (including vertical p-modes), except for those of p-modes, are strongly affected by the poloidal magnetic fields (Fu and Lai 2009). Hence, even if the BH disks have the same kind of disk deformation as that in NS disks (i.e., $m_D = 2$ and $n_D = 0$), it will be natural that the frequency ratio of the c-mode oscillation modes do not have the same characteristics as those in the case of NS disks.

Next, we speculate the origin of the twin HFQPOs. Observations show that the twin HFQPOs in BH X-ray binaries are observed in the transition state from the low/hard state to the high/soft one (Remillard 2005). The transition state will be on the way to transit from ADAFs with strong turbulent magnetic fields to optically thick standard disks with low plasma β . As mass accretion increases in ADAFs, they cannot be in equilibrium states. They will vertically contract by thermal instability due to radiative cooling, leading to low- β disks with coherent strong magnetic fields (Machida et al. 2006). We speculate that in such transition disks with strong poloidal and toroidal magnetic fields, the deformed pattern in disks may be plane-asymmetric, unlike the case of high- β disks considered in low-mass X-ray binaries. In other words, we think that in the intermediate state of the BH X-ray binaries the disk deformation from steady axisymmetric state will be spiral patterns which are asymmetric with respect to equatorial plane (i.e., $n_D = 1$), unlike in the case of NS X-ray binaries where the spiral pattern will be plane-symmetric (i.e., $n_D = 0$).

In the above context, we assume that spiral disk deformations of $m_D = 2$ and $n_D = 1$ are present in the disks of BH X-ray binaries in their intermediate state. That is, we assume the presence of

$$m_D = -2, \quad n_D = 1, \quad \text{and,} \quad \omega_D \sim 0, \quad (13)$$

where we have again adopted $m_D = -2$ instead of $m_D = 2$ for convenience. We then examine what types of oscillations are expected in these deformed disks by the wave-wave resonant processes.

The following set of oscillations satisfy the resonant conditions (5):

$$\text{mode 1: } \quad \text{p - mode oscillations with } (m_1 = 2, n_1 = 0, \omega_1), \quad (14)$$

$$\text{mode 2: } \quad \text{c - mode oscillations with } (m_2 = 0, n_2 = 1, \omega_2 \sim -\omega_1). \quad (15)$$

The propagation region of mode 1 is specified by $(\omega_1 - 2\Omega)^2 - \kappa^2 > 0$. This propagation region is divided into two domains. We are interested in the trapped oscillations in the region of $\omega_1 < 2\Omega - \kappa$ (see figure 6). The waves in this propagation region have negative energy, $E_1 < 0$, since the waves are inside the corotation radius of $\omega_1 = 2\Omega$ (see also figure 6). Hence, we have $E_1/\omega_1 < 0$. The propagation region of mode 2 is specified by $\omega_2^2 - \Omega_\perp^2 > 0$. We are interested in the oscillations in region of $\omega_2 < -\Omega_\perp$ (see figure 6). The wave energy of this oscillation mode is positive, since the wave is axisymmetric, i.e., $E_2 > 0$. Hence, we have $E_2/\omega_2 < 0$, since $\omega_2 < 0$. This consideration shows that the above two oscillations of mode 1 and mode 2 are resonantly excited, since $(E_1/\omega_1)(E_2/\omega_2) > 0$. The propagation region of mode 2 has no definite outer boundary. Hence, as in the case of kHz QPOs the oscillation of mode 2 will not be clearly observed. The oscillation of mode 1 will correspond to the lower frequency one of a twin HFQPOs in black-hole sources, if the oscillation mode is reflected back around r_{in} .

The higher frequency oscillation of a twin HFQPOs in black-hole sources will be the mode 1 of the following set of resonant oscillations under the disk deformation given by (13):

$$\text{mode 1: } \quad \text{p - mode oscillations with } (m_1 = 3, n_1 = 0, \omega_1), \quad (16)$$

$$\text{mode 2: } \quad \text{c - mode oscillations with } (m_2 = -1, n_2 = 1, \omega_2 \sim -\omega_1). \quad (17)$$

Based on arguments similar to those in the case of $m_1 = 2$, we consider the trapped oscillation in the region of $\omega_1 < 3\Omega - \kappa$ as mode 1, and the oscillation in the region of $\omega_2 < -\Omega - \Omega_\perp$ as mode 2. The above-mentioned two modes satisfy the instability condition, $(E_1/\omega_1)(E_2/\omega_2) > 0$. We suppose that the mode 1 mentioned here is the upper frequency QPO of the twin HFQPOs. It is interesting to note that the frequency ratio of the above two mode 1 oscillations (the oscillation with $m_1 = 2$ and that of $m_1 = 3$) is close to 2 : 3 and depends little on disk models (disk temperature) in the case of $a_* = 0$, if they are reflected back around r_{in} (Lai and Tsang 2009, see also figure 7.2 of Kato (2016)).

We should further notice that there is the idea that the cause of HFQPOs in black-hole

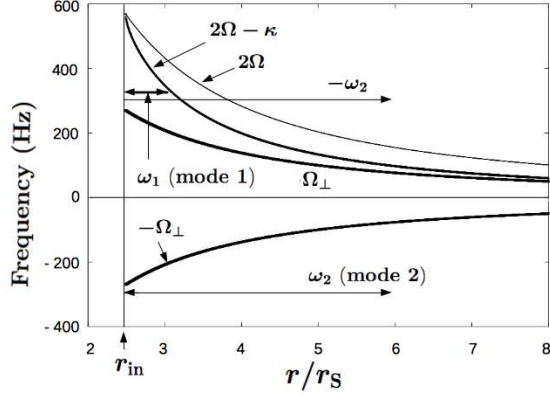


Fig. 6. Schematic figure showing the propagation region of a two-armed p-mode oscillation ($m = 2$, $n = 0$, called mode 1) and the propagation region of the resonantly coupled axisymmetric c-mode oscillations ($m = 0$, $n = 1$, called mode 2). The propagation region of mode 1 is limited by the inner edge of the disk, r_{in} , and outside by the radius where $\omega_1 = 2\Omega - \kappa$. That is, the oscillation is trapped and has a discrete frequency. Different from this, the propagation region of mode 2 is limited inside by the radius where $-\omega_2 = \Omega_{\perp}$ (or by r_{in}), but there is no definite outer boundary. That is, the frequency of ω_2 is determined passively by the resonance condition. The curves of Ω_{\perp} , $2\Omega - \kappa$ and 2Ω in this diagram are drawn in the case of spin parameter a_* is 0.3. The ω_1 oscillation presented in this figure corresponds to the lower frequency QPO of twin HFQPOs in BH X-ray binaries. The ω_1 oscillation for the higher QPO is the p-mode oscillation of $m_1 = 3$. In this case the curve corresponding to $2\Omega - \kappa$ is $3\omega - \kappa$ and the curve corresponding to $-\Omega_{\perp}$ is $-\omega - \Omega_{\perp}$. The frequency of the trapped oscillation, ω_1 , in this case is higher than that shown in this figure.

sources may be due to corotation amplification of the non-axisymmetric p-mode oscillations (14) and (16) (Tsang and Lai 2008, Lai and Tsang 2009) (notice that in figure 6 the corotation radius where $\omega = 2\Omega$ is present just outside of the propagation region of ω_1 oscillation).

Acknowledgments

We thank colleagues of M. Machida in the program of high-resolution numerical simulations of black-hole accretion disks, T. Kawashima, Y. Kudoh, Y. Matsumoto, and R. Matsumoto, for their allowing us to use their unpublished results before publication. This research used computational resources of the K computer provided by the RIKEN Advances Institute for Computational Science through the HPCI System Research project (MM:Project ID:hp 180137, hp 190125). This work was supported by JSPS KAKENHI Grant Number 19K03916.

References

- Abramowicz, M. A. 2005, *Astron. Nachr.*, 326, 782
 Belloni, T., Mendez, M. & Homan, J. 2005, *Astron. Astrophys.* 437, 209
 Dewberry, J. W., Latter, H. N., & Ogilvie, G. I. 2018, *MNRAS*, 476, 4085
 Dewberry, J. W., Latter, H. N., & Ogilvie, G. I. 2019a, *MNRAS*, 483, 1609
 Dewberry, J. W., Latter, H. N., & Ogilvie, G. I. & Fromang, S. 2019b, *Astro-ph*, ArXiv 191010696

- Ferreira, B. T., & Ogilvie, G. I., 2008, MNRAS, 386, 2297
- Fu, W., & Lai, D., 2009, *Astrophys. J.* 690, 1386
- Hirose, M., Osaki, Y. 1990, PASJ, 42, 135
- Honma, F., Matsumoto, R., & Kato, S. 1992, PASJ, 44, 529
- Kato, S. 2001, PASJ, 53, 1
- Kato, S. 2003, PASJ, 55, 257
- Kato, S. 2004, PASJ, 56, 24
- Kato, S. 2008, PASJ, 60, 111
- Kato, S. 2011, PASJ, 63, 125
- Kato, S. 2011, PASJ, 63, 861
- Kato, S. 2012a, PASJ, 64, 62
- Kato, S. 2012b, PASJ, 64, 129
- Kato, S. 2013, PASJ, 65, 75
- Kato, S. 2014, PASJ, 66, 24
- Kato, S. 2016, *Oscillations of Disks* (Springer, Tokyo)
- Kato, S., Honma, F., & Matsumoto, R. 1988, MNRAS, 231, 37
- Lai, D., & Tsang, D. 2009, MNRAS, 393, 979
- Li, L. X., Goodman, J., Narayan, R. 2003, *Astrophys. J.*, 593, 980
- Lubow, S. H. 1991, *Astrophys. J.*, 381, 259
- Machida, M., & Matsumoto, R. 2003, *Astrophys. J.* 585, 429
- Machida, M., Nakamura, K., Matsumoto, R., 2006, PASJ, 58, 193
- Machida, M. & Matsumoto, R. 2008, PASJ, 60, 613
- Machida, M. et al. 2020, in preparation
- Matsumoto, R., Kato, S., & Honma, F., 1988, in *Physics of Neutron Stars and Black Holes*, ed. Y. Tanaka (Universal Academic Press, Tokyo), p. 155
- Matsumoto, Y., Asahina, Y., Kudoh, Y., Kawashima, T., Matsumoto, J., Takahashi, H. R., Minoshima, T., Zenitani, S., Miyoshi, T. & Matsumoto, R. 2019, PASJ, 71, 83
- Okazaki, A. T., Kato, S., & Fukue, J. 1987, PASJ, 39, 457
- Oktariani, F., Okazaki, A.T. & Kato, S. 2010, PASJ, 62, 709
- Remillard, R. A. 2005, *Astro. Nachr.*, 326, 804
- Tsang, D. & Lai, D. 2008, MNRAS, 387, 446
- Tsang, D. & Lai, D. 2009, MNRAS, 393, 979

Appendix: Other Instabilities Described by the Wave-Wave Resonant Instability

The wave-wave resonant instabilities resulting from other types of disk deformations are briefly summarized. For simplicity, the cases of no magnetic fields are shown.

i) Warp resonant instability:

This is the case where the unperturbed disk is warped, i.e.,

$$m_D = -1, \quad n_D = 1, \quad \text{and} \quad \omega_D \sim 0. \quad (18)$$

For convenience, we have adopted here $m_D = -1$ without any physical changes by changing the sign of ω_D simultaneously. The set of resonant oscillations in this case is an axisymmetric g-mode oscillation and an one-armed p-mode oscillation:

$$\text{mode 1: } \quad \text{g - mode oscillations with } (m_1 = 0, n_1 = 1, \omega_1 < 0), \quad (19)$$

$$\text{mode 2: } \quad \text{p - mode oscillations with } (m_2 = 1, n_2 = 0, \omega_2 \sim -\omega_1 > 0), \quad (20)$$

where, for convenience, ω_1 has been taken to be negative. The propagation region of the former is specified by $\omega_1^2 - \kappa^2 < 0$, i.e., $-\kappa < \omega_1 < \kappa$. We take a trapped oscillation with $\omega_1 < 0$. The propagation region of the latter oscillations is specified by $(\omega_2 - \Omega)^2 > \kappa^2$, whose propagation region is divided into two parts. What we are interested in is the oscillations in the region of $\omega_2 < \Omega - \kappa$ with $\omega_2 > 0$.

In mode 1 we have $E_1/\omega_1 < 0$, since oscillations are axisymmetric and $\omega_1 < 0$. In mode 2 we also have $E_2/\omega_2 < 0$, since the waves are inside the corotation resonance of $\omega_2 = \Omega$ and $\omega_2 > 0$. The excitation condition (7) is thus satisfied and the above coupled oscillations are excited (Kato 2004, 2008; Ferreira and Ogilvie 2008).

ii) Eccentric resonant instability:

This is the case where the unperturbed disk is eccentric, i.e.,

$$m_D = -1, \quad n_D = 0, \quad \text{and} \quad \omega_D \sim 0. \quad (21)$$

The set of oscillations which have resonant interaction are an axisymmetric g-mode oscillation and an one-armed g-mode oscillation:

$$\text{mode 1: } \quad \text{g - mode oscillations with } (m_1 = 0, n_1 = 1, \omega_1 < 0), \quad (22)$$

$$\text{mode 2: } \quad \text{g - mode oscillations with } (m_2 = 1, n_2 = 1, \omega_2 \sim -\omega_1 > 0). \quad (23)$$

The propagation region of the former oscillations is $-\kappa < \omega_1 < \kappa$. The propagation region of the latter oscillations is $\Omega - \kappa < \omega_2 < \Omega + \kappa$.

In the case of $\omega_1 < 0$, mode 1 has $E_1/\omega_1 < 0$. On the other hand, mode 2 with $\omega_2 \sim -\omega_1 > 0$ has $E_2/\omega_2 < 0$, if it is present in the propagation region inside the corotation radius of $\omega_2 = \Omega$.

Hence, the condition of resonant instability (7) is satisfied. This resonant instability has been studied by Dewberry et. al. (2019a, b). It should be noticed that the mode 2 considered above has the corotation radius within its propagation region, where the wave is damped (Kato 2003, Li et al. 2003). This might bring about no serious effect on the present resonant excitation.

iii) Tidal instability:

In tidally deformed disks, we have the deformation characterized by

$$m_D = -3, \quad n_D = 0, \quad \text{and} \quad \omega_D = -3\Omega_{\text{obs}}^*, \quad (24)$$

where Ω_{obs}^* is the orbital frequency of the secondary star around the primary star. We have again adopted here $m_D = -3$ (and thus $\omega_D < 0$) for convenience. A set of oscillations which have resonant interaction through this deformation are an one-armed p-mode oscillation ($m_1 = 1, n_1 = 0$) and a two-armed p-mode oscillation ($m_2 = 2, n_2 = 0$). That is,

$$\text{mode 1: } \quad \text{p - mode oscillations with } (m_1 = 1, n_1 = 0, \omega_1 > 0), \quad (25)$$

$$\text{mode 2: } \quad \text{p - mode oscillations with } (m_2 = 2, n_2 = 0, \omega_2 > 0). \quad (26)$$

The propagation region of the former oscillations is characterized by $(\omega_1 - \Omega)^2 > \kappa^2$. This propagation region is separated into two: $\omega_1 > \Omega + \kappa$ and $\omega_1 < \Omega - \kappa$. We are interested in the oscillations in the latter propagation region of $0 < \omega_1 < \Omega - \kappa$. The propagation region of the two-armed p-mode oscillations are characterized by $\omega_2 > 2\Omega + \kappa$ and $\omega_2 < 2\Omega - \kappa$. We are interested in the oscillations in the latter propagation region. This situation is shown in, for example, figure 12.1 by Kato (2016).

The former oscillation mode, mode 1, has $E_1/\omega_1 < 0$, since $\omega_1 - \Omega < -\kappa$ and thus $\omega_1 - \Omega < 0$. In the latter mode, mode 2, we have has $E_2/\omega_2 < 0$. Hence, the instability condition (7) is satisfied. This instability has been known as the 3:1 resonance in tidally deformed disks by simulations (Whitehurst 1988) and by theoretical considerations (Hirose and Osaki 1990; Lubow 1991).

It is noted that many other types of tidal instabilities are possible, since tidal waves are not limited to that considered above, if we extend our attention to cases where the orbit of the secondary star is eccentric and not coplanar (e.g., see Kato 2016).